Journal of Inflammation Research Dovepress

Open Access Full Text Article ORIGINAL RESEARCH

A Novelly-Spatiotemporal Characterization of the Disease Course in the MNU-Induced Retinitis Pigmentosa Model

Weiming Yan[1]*, Qiurui He[2,]*, Pan Long[3,]*, Lei Zhang[4], Haiyan Wang[4], Tao Chen[5]

[1]Department of Ophthalmology, Fuzong Clinical Medical College of Fujian Medical University, Dongfang Hospital Affiliated to Xiamen University, Fuzhou, People's Republic of China; [2]Department of Cardiovascular Intervention, The Third Hospital of Zhangzhou, Zhangzhou, People's Republic of China; [3]Department of Ophthalmology, The General Hospital of Western Theatre Command, PLA, Chengdu, People's Republic of China; [4]Department of Ophthalmology, The Shaanxi Eye Hospital, Xi'an People's Hospital (Xi'an Fourth Hospital), Xi'an, People's Republic of China; [5]Center of Clinical Aerospace Medicine, Air Force Military Medical University, Xi'an, People's Republic of China

*These authors contributed equally to this work

Correspondence: Weiming Yan; Tao Chen, Email ywming@fjmu.edu.cn; baiidtf0506@126.com

Objective: With the aids of ophthalmic imaging techniques for animals, the spatiotemporal characterization of MNU-induced retinitis pigmentosa (RP) rats were performed.

Methods: Sprague-Dawley (SD) rats were randomly divided into normal group (N), MNU-low-dose group (L) and MNU-high-dose group (H). Rats in the L and H group were given intraperitoneally injection with 40 and 60 mg/kg of MNU, a kind of alkylating agent, respectively. The body weight, electroretinogram (ERG) and retinal structure were observed on day one (D1), D3, and D7 after MNU administration. FFA, OCT, TUNEL staining, and immunostaining of Iba1 were also performed.

Results: After MNU injection, the weight and ERG amplitudes of rats in both L and H groups decreased gradually, compared to those of the normal group ($P < 0.05$). Fundus imaging revealed enlargement of the optical disc and slightly reduced shadow of retinal vessels in both L and H groups, which were more obvious on D7. No significant morphological changes of retinal vessels were found under FFA. OCT and retinal histological examination revealed that outer nuclear layers (ONL) became thinner gradually in both L and H groups, and disappeared in H group at D7. MNU administration increased the numbers of apoptotic cells and Iba1-positive cells in the retinas gradually, showing a dose-dependent effect.

Conclusion: MNU gradually reduced the ONL thickness and the ERG amplitudes in the MNU-induced RP model revealed by various ophthalmic imaging techniques, along with the increased apoptosis of photoreceptors, the microglia cells activation, which provide indicators for new intervention effect for RP.

Keywords: retinitis pigmentosa, animal model, N-methyl-N-nitrosourea, microglia

Introduction

Retinitis pigmentosa (RP) is a group of genetic disorders that involve a breakdown and loss of cells in the retina. It affects approximately 1 in 4000 individuals worldwide and can result in serious visual impairment or blindness.[1] This progressive degeneration of the retina can lead to vision loss and eventual blindness. Symptoms of RP often begin with decreased night vision and the gradual loss of peripheral vision, eventually leading to tunnel vision or total blindness in severe cases. The causative genes for RP are highly heterogeneous.[2] The exact pathogenesis of this disease is not yet fully understood and clinically it is still lack of effective prevention and treatment measures. Establishing suitable animal models is a necessary condition for the research on the pathogenesis and therapeutic intervention for RP.[3]

MNU, also known as N-methyl-N-nitrosourea, is an alkylating agent originally used in chemotherapy for leukemia.[4] The MNU-induced RP rat model is one of the commonly used animal models in RP research. In the context of MNU-induced RP, the specific degeneration occurs mainly in the outer retinal layers (ONL), particularly the photoreceptor cells (PRs).[5] In greater

Received: 16 April 2024
Accepted: 24 October 2024
Published: 20 November 2024

© 2024 Yan et al. This work is published and licensed by Dove Medical Press Limited. The full terms of this license are available at https://www.dovepress.com/terms.php and incorporate the Creative Commons Attribution – Non Commercial (unported, v3.0) License (http://creativecommons.org/licenses/by-nc/3.0/). By accessing the work you hereby accept the Terms. Non-commercial uses of the work are permitted without any further permission from Dove Medical Press Limited, provided the work is properly attributed. For permission for commercial use of this work, please see paragraphs 4.2 and 5 of our Terms (https://www.dovepress.com/terms.php).

details, the model shows a progressive loss of photoreceptor cells, which can effectively simulate the pathophysiological progression of RP and exhibits distinct spatiotemporal characteristics. Studies have found that MNU can induce mammary cancer in female animals and has been widely used in related research.[6] Subsequently, researchers found that a single intraperitoneal injection of MNU can induce retinal degeneration in rodents, with the damage mainly limited to the photoreceptor cells.[7] The induction of retinal damage by MNU has also been observed in other animal species, including rabbits, zebrafish, etc., showing selective damage to the photoreceptor cells.[8] This model is widely used for RP-related research.

This selective vulnerability of the ONL to MNU-induced damage highlights the model's relevance for understanding the mechanisms underlying photoreceptor degeneration. Specially, the main damaging effect of MNU on photoreceptor cells is attributed to the nitrogen atom, causing instability in the associated carbonyl groups, forming electrophilic groups that bind to nuclear DNA through cross-linking, disrupting DNA transcription and replication, damaging DNA structure, causing DNA breakage, and inhibiting cell division and proliferation. When the body is damaged by MNU, it initiates a stress response to repair the damaged DNA. If the damage is mild, it can to some extent prevent further action, maintaining the overall normal structure and function of the cells; if the damage is severe, it leads to cell death.[9] The selective action of MNU on the photoreceptor cells in the retina may be related to the active metabolism of these cells, abundant mitochondria, high oxygen consumption, and continuous renewal of membrane disks.[10]

Microglial cells are the resident immune cells of the central nervous system, including the retina.[11] They could undergo activation and contribute to the progressive degeneration of retinal cells, particularly photoreceptors. Based on previous research, this study, combined with various small animal ophthalmic imaging equipments, observeed a novelly-spatiotemporal characterization of the disease course characteristics of the MNU-induced RP rat model. We also focused on activation of microglial cells in the model, providing experimental indicators for exploring new interventions for RP.

Materials and Methods

Experimental Subjects

Healthy SPF-grade male SD rats (8–9 weeks old, purchased from the Experimental Animal Center of the Air Force Medical University) were acclimated to the following conditions: room temperature of 22–25°C, with a 12/12-hour light/dark cycle, for 3 days with ad libitum access to water. The use of experimental animals followed the relevant regulations of ARVO and the Regulations on the Management of Experimental Animals in China. The ethical and legal approval was obtained from the Animal Care and Use Committee of the Air Force Medical University and the Fuzong Clinical Medical College of Fujian Medical University.

Preparation of MNU Solution

Firstly, calculated the required amount of MNU, the alkylating agent, (for example, to induce RP model at a dose of 60 mg/kg in 10 SD rats weighing 300 g each, the amount of MNU needed would be MNU = 60×10 × 0.3 = 180 mg). Then, calculated the corresponding concentration of the MNU solution for injection at a volume of 10 mL/kg, as well as the required volume of physiological saline (for instance, if MNU was administered at 60 mg/kg and injected at a volume of 10 mL/kg, the corresponding concentration of the MNU solution should be 6 mg/mL, and 180 mg of MNU would require a volume of physiological saline of 180/6 = 30 mL). Finally, added an amount of ice acetic acid at a concentration of 0.05% based on the volume ratio (for example, if preparing a MNU solution requiring 30 mL of physiological saline, then 30×0.05% = 0.015 mL = 15 μL of ice acetic acid was needed to be added). Mixed thoroughly to form the solution, stored it at 4°C for later use, and prepared it immediately before use.

Experimental Grouping and MNU-Induced RP Modeling

Thirty-six SD rats were randomly grouped as follows: The rats were numbered starting from "1" and weighed simultaneously. After sorting by weight in ascending order, a set of random numbers (two digits) was selected from Appendix 15 of the Statistical Textbook (People's Medical Publishing House, 3rd Edition). These random numbers were then assigned to the rats according to their corresponding weight-based numbers, resulting in 36 random numbers. Starting from the beginning, every three sequentially numbered rats were sorted based on the corresponding random number, resulting in groups 1, 2, and 3, which corresponded to the normal group (N), the low-dose MNU group (L), and

the high-dose MNU group (H), with each group comprising 12 rats. Rats in the low-dose and high-dose MNU groups were administered MNU at doses of 40 mg/kg and 60 mg/kg, respectively, via intraperitoneal injection, while the normal group received no treatment. Relevant indicators were measured at 1, 3, and 7 days after modeling, followed by molecular biological indicators detection using eye specimens.

Weight Measurement

At 1, 3, and 7 days after modeling, the weight of each group of rats was recorded in grams.

ERG Measurement

Rats were anesthetized via intraperitoneal injection with a combination of pentobarbital sodium and dormicum (at a dosage of 0.3 mL/kg and approximately 0.05 mL per rat, respectively). Based on the standardized protocol for small animal visual electrophysiology established in our laboratory, the ISCEV five-item ERG test was conducted, including the dark-adapted 0.01 response, dark-adapted 3.0 response, dark-adapted Ops wave response, light-adapted 3.0 response, and light-adapted Flicker response. The right eye was tested uniformly. Data for each rat was recorded separately, and the amplitude values (μV) of the dark-adapted 3.0 ERG and light-adapted 3.0 ERG b-waves were calculated. The specific experimental procedures were the same as previously reported.[12] The rats' corneas were kept moist during the experiment, and after the test, levofloxacin eye drops were promptly administered to prevent infection.

Slit Lamp Photography of the Ocular Surface

Following the ERG assessment, a slit lamp was used to adjust the slit to a narrow shape (approximately 5 mm). The right eye of the rat was placed on a small animal support platform, and after pupil dilation, the slit lamp light band was positioned at the center of the cornea. Using the central retinal reflex method, photographs were taken and observed at 25x magnification.

Fundus Photography, OCT, and FFA Examination

Under anesthesia and pupil dilation, the rat was placed on a small animal support platform for angle adjustment. Fundus photography and OCT imaging of the rat's eye were conducted according to the methods described previously,[13] with attention paid to maintaining corneal moisture. The OCT images were analyzed using the OCT image analysis software (version 2.0, Optoprobe, Canada) provided with the OCT device, measuring the distance from the retinal pigment epithelium (RPE) to the outer plexiform layer (OPL) at 800 μm from the optic disc. Fluorescein fundus angiography (FFA) was performed using a Heidelberg retinal angiograph. Following the methods, 10% sodium fluorescein (0.1 mL/100 g) was injected intraperitoneally, and after waiting approximately 1 to 2 minutes, the laser probe was aimed at the rat's eyeball for focusing until a clear retinal image was obtained. Subsequently, the instrument was switched to blue light mode (FFA) to observe the retinal vascular imaging. Sequential observations were made in the order of temporal superior, temporal inferior, nasal superior, and nasal inferior, with the optic disc as the center for subsequent analysis.

Collection of Eyeball Specimens

After ophthalmic morphological examination, rats from each group and time point were euthanized by cervical dislocation. The right eyeballs were placed in a mixed fixative for histopathological, immunofluorescence staining, and TUNEL staining, while the left eyeballs were frozen in liquid nitrogen for subsequent analysis.

Retinal Histopathological Paraffin Sections and HE Staining

After fixation of the eyeballs at 4°C for 2 hours, the cornea of each group of rat eyeballs was cut with corneal scissors, and then further fixed for 24 hours. Retinal histopathological paraffin sections with HE staining was performed (same method as before), and photographs were taken using a microscope. For each HE-stained section, the thickness of the corresponding ONL was measured at the central region (approximately 200 μm from the optic nerve), the mid-peripheral region (approximately 2000 μm from the optic nerve), and the peripheral region (approximately 4000 μm from the optic

nerve). Three HE-stained section specimens were taken for each time point in each group of rats, and the average values were recorded.

Retinal Iba1 Immunofluorescence Staining

The method for immunofluorescence staining of retinal Iba1 in rats was the same as before. Fluorescence microscope images were taken, and photographs of the central field of the retina (×400) were captured. The number of Iba1-positive cells in the outer retina (outside the outer plexiform layer), inner retina (inside the outer plexiform layer), and the entire retina were counted. Three specimens were used for each time point in each group, and the average values were recorded.

TUNEL Staining Paraffin Sections

Retinal sections were routinely dewaxed to water, followed by immersion in preheated trypsin solution at 37°C for 30 minutes. After washing with PBS, a mixture of A and B from the TUNEL assay kit, in a 1:9 ratio, was used at approximately 50 μL per tissue, and was prepared as needed for the required volume. Negative control samples only received 50 μL of B solution, and were then incubated at room temperature for 2 hours. After further washing with PBS, DAPI was applied at room temperature for 10 minutes, followed by another round of PBS washing, and finally mounting with 50% glycerol. Fluorescence microscope images were taken, and high magnification views (×400) of the central region (200 μm from the optic nerve), mid-peripheral region (2000 μm from the optic nerve), and peripheral region (4000 μm from the optic nerve) of the retina were photographed for counting TUNEL-stained positive cells. Three specimens were used for each time point in each group, and the average values were recorded.

Statistical Analysis

SPSS 16.0 software was used for data statistical analysis. The data from the experiment were found to be normally distributed, represented as mean ± standard deviation. One-way analysis of variance (ANOVA) was employed for intergroup comparison, using LSD-*t* test (for homogeneity of variance) or Dunnett's T3 test (for inhomogeneity of variance), with $P < 0.05$ indicating statistical significance. Graphs were created using GraphPad 5.01 software.

Result

Effect of MNU on Body Weight in Rats

Before modeling, there were no statistically significant differences in body weight among the normal group, MNU low-dose group, and MNU high-dose group of rats ($P > 0.05$). Within one week after MNU injection, the body weight of rats in the MNU low-dose group and MNU high-dose group gradually decreased, in contrast to the gradual increase observed in the body weight of rats in the normal group. At D1, D3, and D7, there were significant differences in body weight between the MNU low-dose group or MNU high-dose group and the normal group ($P < 0.01$). At D7, the body weight of rats in the MNU low-dose group showed a tendency to rebound, while the MNU high-dose group continued to exhibit a decreasing trend (Figure 1).

Effect of MNU on the Retinal Function in Rats

Dark adaptation 3.0 ERG response mainly reflects the function of the retinal rod system, while light adaptation 3.0 ERG response mainly reflects the function of the cone system. The ERG results showed that after modeling, the amplitude of the b-wave in the light adaptation 3.0 ERG response did not decrease significantly in the D1, low-dose MNU group, and high-dose MNU group rats, with no statistically significant difference compared to the normal group rats ($P > 0.05$). However, at this time, the amplitude of the b-wave in the dark adaptation 3.0 ERG response decreased significantly, with a statistically significant difference compared to the normal group (MNU low-dose group vs normal group, $P < 0.05$; MNU high-dose group vs normal group, $P < 0.01$). On D3 and D7, the visual function of rats in the low-dose MNU group and high-dose MNU group gradually decreased, with the b-wave amplitude in the low-dose MNU group rats being higher than that in the high-dose MNU group, and the difference was statistically significant ($P < 0.05$) (Figure 2).

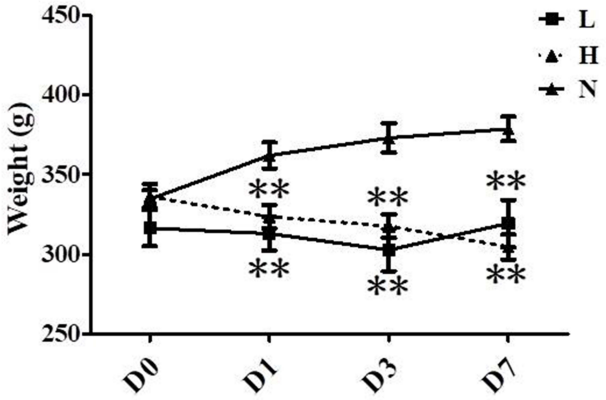

Figure 1 Effect of MNU on body weight in rats. Plot of quantitative analysis of body weight in rats of each group within 1 week after MNU injection. Both low dose (40 mg/kg) and high dose (60 mg/kg) of MNU gradually decreased rats' body weight. N: normal group; L: MNU-low-dose group; H: MNU-high-dose group; **: $P < 0.01$ vs normal group.

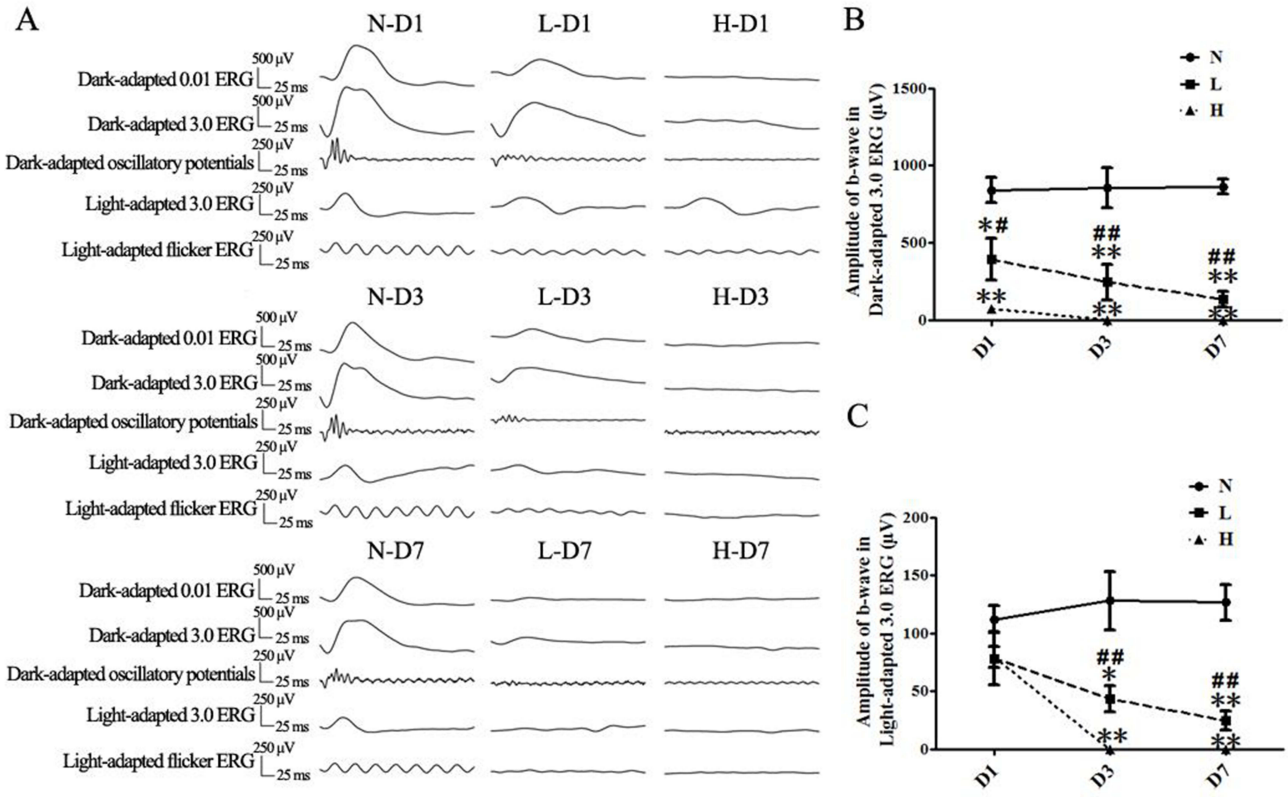

Figure 2 Effect of MNU on the retinal function in rats. Typical ERG waveforms (**A**) and statistical analysis of the b-wave amplitude in Dark-adapted 3.0 ERG (**B**) and Light-adapted ERG (**C**) on D1, D3 and D7 after MNU injection. MNU of low dose (40 mg/kg) and high dose (60 mg/kg) significantly reduced the amplitudes of ERG responses gradually. The amplitude of ERG in the MNU-low-dose group was higher than that in the MNU-high-dose group. The MNU has a dose-dependent effect of the retinal function. N: normal group; L: MNU-low-dose group; H: MNU-high-dose group. *(**): $P < 0.05$ ($P < 0.01$) vs normal group; #(##): $P < 0.05$ ($P < 0.01$) vs MNU-high-dose group.

Effect of MNU on the Structure of the Rat Ocular Fundus and Retinal Vessels

After intraperitoneal injection of MNU on Day 3, the dilated pupils of rats were observed under a slit lamp to examine the red reflex of the fundus. The results indicated that in the control group, a red reflex was visible in the fundus of the rats, while in the low-dose MNU group and high-dose MNU group, the fundus response appeared pale (Figure 3A). Fundus photography revealed that after MNU injection, the optic disc contour of the fundus in the low-dose and high-

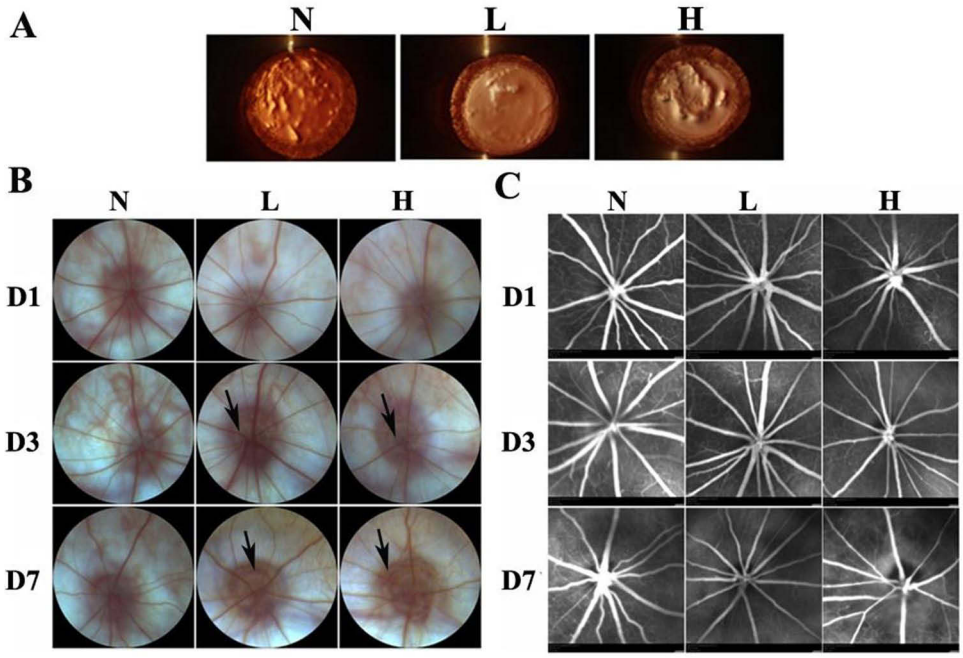

Figure 3 Effect of MNU on the structure of the rat ocular fundus and retinal blood vessels. (**A**) Typical images of slit-lamp in the rats all groups at D3 after MNU injection. Typical images of ocular fundus (**B**) and FFA (**C**) at D1, D3, and D7 after MNU administration. MNU reduced the reflection light of ocular fundus and widened the optic disc contour on the fundus. There were no significant changes in retinal vascular structure, such as vessel defect and leakage of fluorescence, in rats of MNU-low or high dose group. N: normal group; L: MNU-low-dose group; H: MNU-high-dose group; Arrows: Enlargement of fundus.

dose MNU groups gradually widened, especially noticeable by Day 7, with a slight decrease in retinal vessel shadows (Figure 3B). Fluorescein fundus angiography (FFA) examination of the low-dose and high-dose MNU groups showed no leakage of fluorescein sodium or neovascularization, suggesting no significant changes in retinal vascular structure (Figure 3C).

Effect of MNU on the Retinal Morphology in Rats

Optical coherence tomography (OCT) results demonstrated a gradual disappearance of the outer nuclear layer (ONL) in the retinas of rats in the low-dose and high-dose MNU groups after MNU injection. In normal rats, the ONL appeared as a low-density shadow (black), whereas in the low-dose and high-dose MNU groups, the ONL appeared as a high-density shadow (white) after MNU injection, forming a high-density sheet shadow between the outer plexiform layer (OPL) and retinal pigment epithelium (RPE), including the inner and outer segments (ie, IS/OS), making it difficult to clearly distinguish the boundary of the ONL. Quantitative analysis of the distance from RPE to OPL in the retina revealed that on Days 1, 3, and 7 after modeling, this distance gradually decreased in the retinas of rats in the low-dose and high-dose MNU groups compared to the control group, with statistically significant differences ($P < 0.05$). Additionally, the distance from RPE to OPL in the retinas of rats in the high-dose MNU group was smaller than that in the low-dose MNU group, with statistically significant differences evident by Day 7 ($P < 0.05$) (Figure 4). Histopathological examination of the retinas was consistent with the OCT findings. After MNU injection, the ONL in the central, mid-peripheral, and peripheral regions of the retinas gradually disappeared in the low-dose and high-dose MNU groups. On Day 1 after modeling, there was no statistically significant difference in ONL thickness between the low-dose MNU group and the control group ($P > 0.05$), while in the high-dose MNU group, there was a statistically significant difference in ONL thickness compared to the control group in the central and mid-peripheral regions of the retina ($P < 0.05$). By Day 7, almost all of the ONL had disappeared in the entire retina of rats in the high-dose MNU group, while in the low-dose MNU group, the ONL had completely disappeared in the central and mid-peripheral regions, with some residual structure in the peripheral region. There were no apparent changes in the inner nuclear layer (INL) or ganglion cell layer (GCL) of the retina (Figure 5).

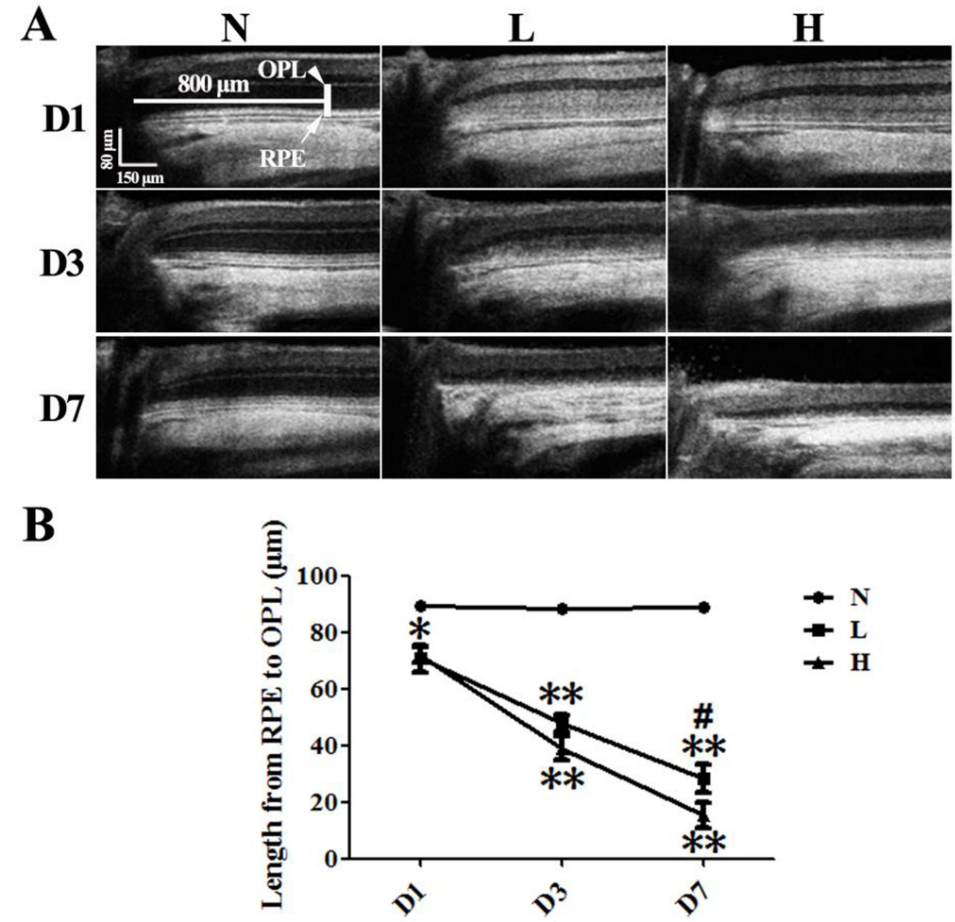

Figure 4 Effect of MNU on the retinal morphology in-vivo in rats. Typical retinal OCT images of rats in D1, D3 and D7 after MNU administration (**A**), and statistical analysis of the length from RPE to OPL in retinas (**B**). MNU administration turned the low density appearance of ONL in OCT images into high density shadow. The length from RPE to OPL was gradually decreased after MNU administration with a dose-dependent effect. N: normal group; L: MNU-low-dose group; H: MNU-high-dose group. * (**): $P < 0.05$ ($P < 0.01$) vs normal group; #: $P < 0.05$ vs MNU-high-dose group.
Abbreviations: OPL, outer plexiform layer; RPE, retinal pigment epithelium.

Effect of MNU on the Photoreceptor Apoptosis in Rat Retinas

TUNEL staining is used to label apoptotic cells, and the dye TdT enzyme binds to fragmented DNA fragments, resulting in a green color (as used in this experiment). TUNEL staining results showed no TUNEL-positive cells in the retinas of rats in the normal group. On Day 1 and Day 3 after modeling, there were significant statistical differences in TUNEL-positive cells between the normal group and the MNU low-dose group, as well as the MNU high-dose group ($P < 0.01$, not indicated in the figure). On Day 1 after modeling, there were a significant number of TUNEL-positive cells in the central, mid-peripheral, and peripheral regions of the retinas of rats in the MNU high-dose group, while in the MNU low-dose group, TUNEL-positive cells were present in the central and mid-peripheral regions of the outer nuclear layer (ONL), and no positive cells were observed in the peripheral region. The number of TUNEL-positive cells in the ONL of the MNU high-dose group was greater than that in the MNU low-dose group, with a statistically significant difference ($P < 0.05$). On Day 3 after modeling, the number of TUNEL-positive cells increased in the MNU low-dose group. In the central region of the ONL, almost all of the ONL had disappeared in the MNU high-dose group, with only a small number of positive cells remaining, which was fewer than in the MNU low-dose group ($P < 0.01$). The number of TUNEL-positive cells increased in the mid-peripheral and peripheral regions of the retina in the MNU high-dose group, with a statistically significant difference compared to the MNU low-dose group ($P < 0.01$). On Day 7 after modeling, no TUNEL-positive cells were observed in the retinas of rats in the MNU low-dose group or the MNU high-dose group (Figure 6).

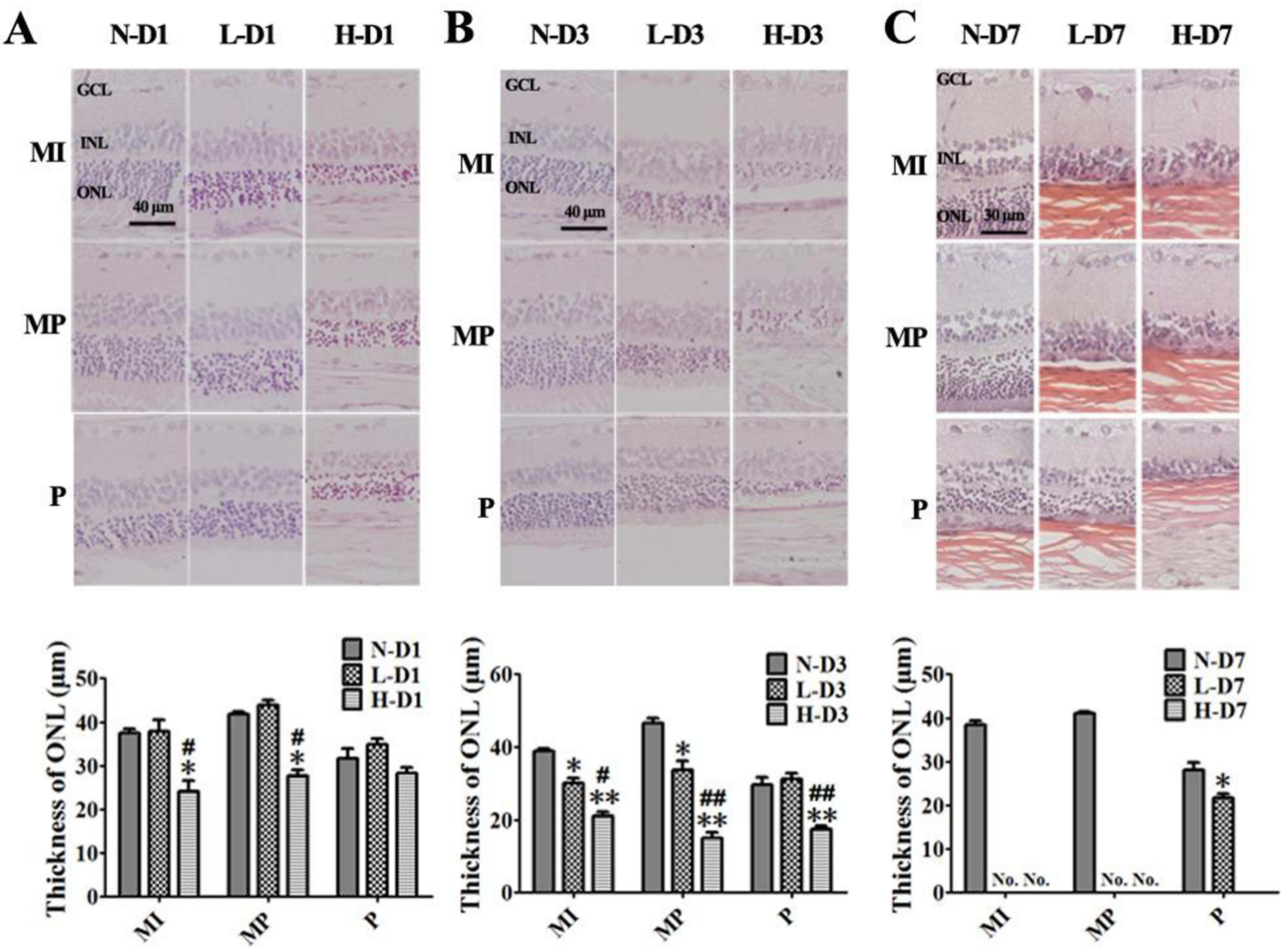

Figure 5 Effect of MNU on the retinal morphology ex-vivo in rats. Typical retinal paraffin sections with HE staining of the rats in each group and the statistical analysis of the ONL thickness at the central (MI), mid-peripheral (MP) and peripheral (P) retinas at D1 (**A**), D3 (**B**), and D7 (**C**) after MNU administration. MNU significantly reduced ONL thickness gradually, with the central part of the retinas involved at first, and then the peripheral part of the retinas. The ONL thickness in the MNU-high-dose group was significantly reduced compared to the MNU-low-dose group. N: normal group; L: l MNU-low-dose group; H: MNU-high-dose group. * (**): $P < 0.05$ ($P < 0.01$) vs normal group; # (##): $P < 0.05$ ($P < 0.01$) vs MNU-low-dose group.

Abbreviations: ONL, outer nuclear layer; INL, inner nuclear layer; GCL, ganglion cell layer; MI, Middle retina; MP, midperipheral retina; P, peripheral retina; No, None.

Effect of MNU on Microglia Activation in the Retina of Rats

After modeling, the number of Iba1-positive cells in the retinas of rats in the MNU low-dose group and MNU high-dose group gradually increased, mainly in the outer retina. The difference in the number of Iba1-positive cells in the retinas between the MNU groups and the normal group was statistically significant ($P < 0.05$). On Day 3 after modeling, the number of microglial cells in the outer retina significantly increased in both the MNU low-dose group and MNU high-dose group, and the difference compared to the normal group was statistically significant ($P < 0.01$). The activated microglial cells exhibited a larger size and reduced peripheral processes, resembling an amoeboid shape. At this time, the MNU high-dose group had a higher number of Iba1-positive cells in the retina compared to the low-dose group ($P < 0.05$). On Day 7 after modeling, there were almost no Iba1-positive cells in the outer retina of both the MNU low-dose group and MNU high-dose group, and the difference compared to the normal group was not statistically significant ($P > 0.05$). At this time, the majority of Iba1-positive cells were located in the inner retina, and the difference compared to the normal group was statistically significant ($P < 0.05$) (Figure 7).

Discussion

Actually, there have been researches on the MNU-induced retinal degeneration animal model. Our study's innovation lied in the application of multimodal ophthalmic examination methods, along with supplementary explorations from aspects

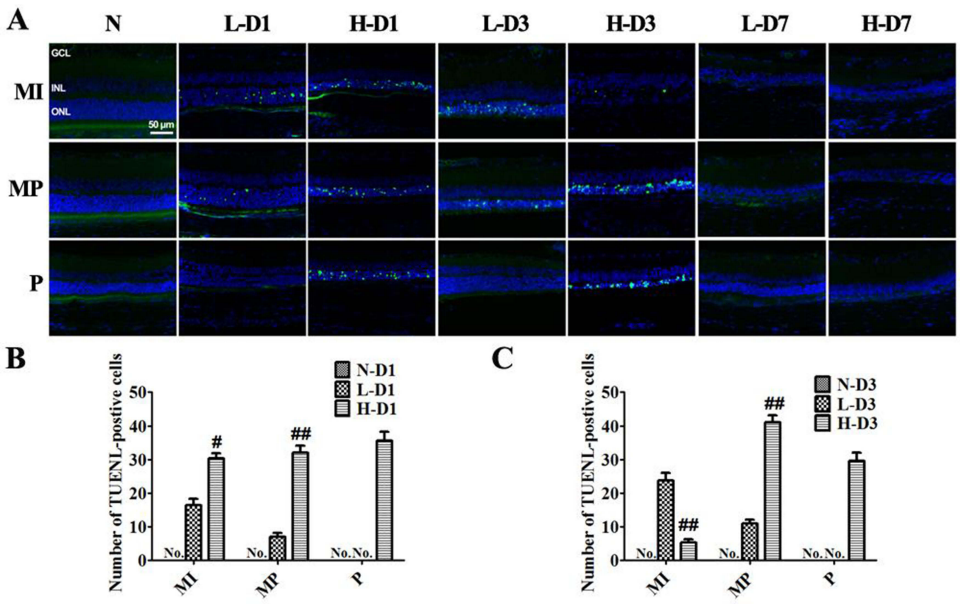

Figure 6 Effect of MNU on the photoreceptor apoptosis in rat retinas. Typical images of TUNEL staining of the retinas in rats of each group and the statistical analysis of the TUNEL-positive cells number at the central, mid-peripheral and peripheral retinas at D1 (**A**), D3 (**B**), and D7 (**C**) after MNU administration. MNU induced cell apoptosis in the ONL of the rat retina, and the number of apoptotic cells in the MNU-high-dose group was much higher than that in the MNU-low-dose group before the ONL disappeared, with the difference being statistically significant. N: normal group; L: l MNU-low-dose group; H: MNU-high-dose group. # (##): $P < 0.05$ ($P < 0.01$), compared to the MNU-low-dose group.

Abbreviations: ONL, outer nuclear layer; INL, inner nuclear layer; GCL, ganglion cell layer; No, None.

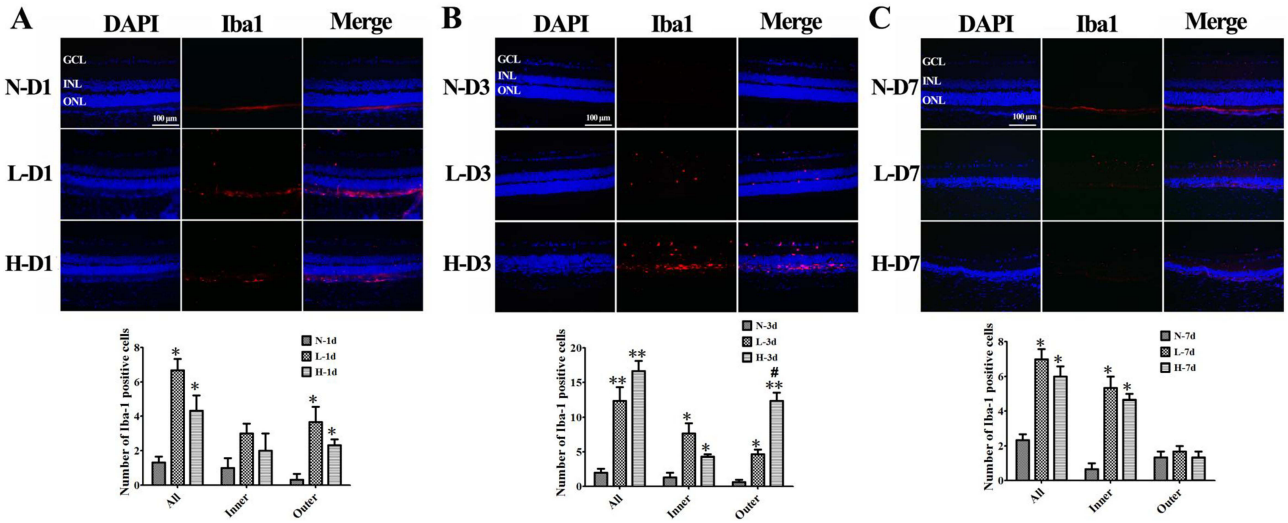

Figure 7 Effect of MNU on microglia activation in the retina of rats. Typical images of Iba1 immunostaining in the rat retina of each group and the statistical analysis of the Iba1-positive cells number in the retinas at D1 (**A**), D3 (**B**), and D7 (**C**) after MNU administration. MNU activated the microglia cells and increased the number of Iba1-positive cells in the retina of rats, reaching a peak at D3. The number of Iba1-positive cells in MNU-high-dose group was higher than that in the MNU-lower dose group, with a significant difference. N: normal group; L: MNU-low-dose group; H: MNU-high-dose group; * (**): $P < 0.05$ ($P < 0.01$) vs normal group; #: $P < 0.05$ vs MNU-low-dose group.

Abbreviations: ONL, outer nuclear layer; INL, inner nuclear layer; GCL, ganglion cell layer.

such as microglial activation. By applying the ophthalmic inspection equipment, we found out that MNU had no significant effect on the retinal vasculature of rats. The disappearance of the red reflex and the enlargement of the optic disc contour in the fundus may be due to the disappearance of retinal photoreceptor cells and the thinning of the retina. This provides further evidence of the selective damaging effect of MNU on photoreceptor cells. An appropriate dose of MNU can cause a progressive loss of retinal photoreceptor cells and a gradual decline in retinal function until

complete loss.[14] Generally, the literature often uses a dose of 60 mg/kg; and there are also studies indicating that 40 mg/kg is the minimum dose to cause retinal damage,[14,15] which may be related to different experimental conditions. In this part of the experiment, we used two doses of MNU to induce retinal damage models in rats, and observed through retinal morphological and functional indicators, finding that both doses could significantly damage photoreceptor cells. This damaging effect progressed from the central part of the retina to the peripheral part, and the damaging effect of the low dose (40 mg/kg) MNU on the peripheral part of the retina was not significant. What is interesting, we found that the rats of the low-concentration group returned to normal weight at D7, but the thickness of ONL in the retina continued to decline. The MNU itself has a certain sensitivity and specificity for ONL in the retina. MNU primarily affects tissues with a higher metabolic rate, such as the retina, where its affinity is stronger. Therefore, even though the low dose of MNU has minimal systemic effects, it could still continue to impact retinal function and structure.

Retinal functional ERG testing found that after the action of MNU, the amplitude of the rod system decreased earlier and more significantly than that of the cone system, suggesting that this model first damages rod cells and then cone cells, consistent with previous research reports,[16] and consistent with the trend in human RP diseases where rod cells undergo apoptosis first, followed by involvement of cone cells.[17] Studies have found that in animal models of light-induced retinal damage, the degree of decrease in rod system amplitude is more significant than that of the cone system, indicating severe damage to rod cells. However, in the rat ischemia-reperfusion injury model, we found that the degree of damage to the cone system after modeling occurred earlier and was more severe than that of the rod system (data not yet published). This suggests that rod and cone cells may have different sensitivities to various damaging factors (chemical, physical, ischemic-hypoxic, etc).

In addition, in this part of the experiment, we systematically observed the changes in the rat retina after MNU injury using small animal OCT imaging technology. We found that the outer nuclear layer (ONL) in the OCT images transitioned from a normal low-density image (black) to a high-density image (white). Optically, this is caused by an increase in tissue cell scattering index (dispersion value). Similar phenomena have been observed using OCT in animal models of light-induced retinal damage[18] and other RP model animals.[19] This is possibly related to changes in the nuclear morphology of ONL cells. The principle of OCT imaging is based on receiving reflected light and scattered light. When there is more reflected light on the tissue surface, the OCT device receives more reflected light, resulting in a high-density image. Another factor is related to the scattering of light within the tissue structure. Changes in cellular morphology and structure can alter their scattering structure. The degree of scattering is determined by the density and size of particles between tissues; the greater the particle density, the stronger the scattering.[20] The main mechanism of ONL cell death in MNU is through apoptosis, which involves cell shrinkage, nuclear condensation, followed by nuclear fragmentation and dissolution.[21] These changes may cause an increase in optical reflection and scattering index, leading to the “white shadow” appearance of ONL in OCT images.This part of the experiment also confirmed the involvement of apoptosis in MNU-induced ONL damage through TUNEL staining. However, TUNEL staining revealed that apoptotic positive cells did not occupy the entire ONL, while the OCT images showed the entire layer of ONL appearing as a “white shadow”. TUNEL staining only labels degraded DNA fragments in late-stage apoptotic cells and cannot mark early changes in the apoptosis process (including morphological changes on the cell membrane and nucleus). Therefore, the changes in ONL density shadows in OCT images may serve as an indicator for the early detection of cell apoptosis. Whether these changes in cell density shadows observed in OCT are limited to ONL or can also be observed in the inner nuclear layer (INL) and ganglion cell layer (GCL) awaits further verification in different models.

Microglias are surveillance cells in the retina that are normally in a non-activated state. However, when they are stimulated by injury or changes in the surrounding microenvironment, their morphology changes from a non-activated elongated structure to an activated amoeboid structure.[10] Iba1 is a calcium ion channel expressed in microglia, and its expression increases when microglia are activated. It is involved in processes such as membrane edge fluctuations and migration.[22] Immunofluorescence staining using Iba1 revealed that in normal rat retinas, there are only a few non-activated microglia in the inner retinal layer. After MNU injection, the cell bodies of microglia in the retina enlarge and migrate towards the outer retinal layer, and their number gradually increases over time. This indicates that microglia are involved in the pathogenesis of MNU-induced RP in rats, which is consistent with reports on other RP animal model.[23]

The activation of microglia may be due to the damaging effect of MNU on photoreceptor cells, leading to the release of inflammatory and cytokine factors that activate microglia.

Indeed, in human RP, the progression is usually relatively slow, typically starting with peripheral retinal damage before affecting the central retina. In this animal model, however, the progression is much faster, usually within about seven days, with the central retina being affected first, followed by the peripheral retina. Although the human RP has a longer progression, the loss of photoreceptor cells is thought to be due to apoptosis. Our experimental results also show the apoptosis of photoreceptor cells through TUNEL staining, suggesting that these findings are of certain similarity to that of human RP. Additionally, the use of different concentrations of MNU in our model is aimed at exploring the progression speed of the disease and the time window for pharmacological intervention. In our previous studies, we conducted some exploratory intervention experiments, administering treatment either simultaneously with MNU injection or prior to it. This provides clinical evidence suggesting that early intervention may be beneficial for patients with a family history of RP or for those who have been diagnosed with RP.

In this study, a successful modeling of the MNU-induced rat RP model was achieved, providing a novelly-spatiotemporal characterization of the disease course in retinal morphology and function by various ophthalmic imaging techniques. The central retina was affected earlier compared to the peripheral retina, and rod cells were affected earlier compared to cone cells. Furthermore, activated microglia was observed in this model. These findings provide indicators for subsequent investigations into the intervention effects and mechanisms of new treatments for RP.

Data Sharing Statement

The datasets used and/or analyzed during the current study were available from the corresponding author on reasonable request.

Acknowledgement

The authors would like to express their gratitude to Professor Dongliang Li from the Fuzong Clinical Medical College of Fujian Medical University, for his support and guidance in the research approach of this study, as well as for sponsoring and providing great assistance in the funding of the project.

Funding

This work was supported by the grants from the Postdoctoral Science Foundation of the Fuzhou General Hospital (Grant number: 48678), the Key Scientific Research Project of Fuzong Clinical Medical College of Fujian Medical University (Project number: 2022ZD04), the Natural Science Foundation of Fujian Province, China (No. 2024J011148), the Natural Science Foundation of Zhangzhou City, China (No. ZZ2024J57), the Xi'an Science and Technology Project (24YXYJ0091), and the General Cultivation Project of Municipal Health Commission in Xi'an, China (2024ms18).

Disclosure

Weiming Yan, Qiurui He and Pan Long are co-first authors. The authors declared no potential conflicts of interest with respect to the research, authorship, and/or publication of this article.

References

1. Wu Y, Wan X, Zhao D, et al. AAV-mediated base-editing therapy ameliorates the disease phenotypes in a mouse model of retinitis pigmentosa. *Nat Commun*. 2023;14(1):4923. doi:10.1038/s41467-023-40655-6
2. Kanan Y, Hackett SF, Hsueh HT, Khan M, Ensign LM, Campochiaro PA. Reduced inspired oxygen decreases retinal superoxide radicals and promotes cone function and survival in a model of retinitis pigmentosa. *Free Radic Bio Med*. 2023;198:118–122. doi:10.1016/j.freeradbiomed.2023.01.021
3. Ostrovskaia LA, Korman DB, Bliukhterova NV, Fomina MM, Rykova VA. Taxotere and methylnitrosourea: experimental appraisal of combination chemotherapy. *Vopr Onkol*. 1999;45(4):429–433.
4. Tao Y, Chen T, Liu B, et al. The neurotoxic effects of N-methyl-N-nitrosourea on the electrophysiological property and visual signal transmission of rat's retina. *Toxicol Appl Pharmacol*. 2015;286(1):44–52. doi:10.1016/j.taap.2015.03.013
5. Mohd NS, Idris F, Jaafar H. Cellular and molecular changes in MNU-induced breast tumours injected with PF4 or bFGF. *Asian Pac J Cancer Prev*. 2017;18(12):3231–3238. doi:10.22034/APJCP.2017.18.12.3231

6. Herrold KM. Pigmentary degeneration of the retina induced by N-methyl-N-nitrosourea. An experimental study in Syrian hamsters. *Arch Ophthalmol*. 1967;78(5):650–653.
7. Rosch S, Werner C, Muller F, Walter P. Photoreceptor degeneration by intravitreal injection of N-methyl-N-nitrosourea (MNU) in rabbits: a pilot study. *Graefes Arch Clin Exp*. 2017;255(2):317–331. doi:10.1007/s00417-016-3531-7
8. Watanabe Y, Nakajima K, Mizukami S, et al. Differential effects between developmental and postpubertal exposure to N-methyl-N-nitrosourea on progenitor cell proliferation of rat hippocampal neurogenesis in relation to COX2 expression in granule cells. *Toxicology*. 2017;389:55–66. doi:10.1016/j.tox.2017.06.013
9. Furukawa A, Koriyama Y. A role of heat shock protein 70 in photoreceptor cell death: potential as a novel therapeutic target in retinal degeneration. *CNS Neurosci Ther*. 2016;22(1):7–14. doi:10.1111/cns.12471
10. Karlstetter M, Scholz R, Rutar M, Wong WT, Provis JM, Langmann T. Retinal microglia: just bystander or target for therapy? *Prog Retin Eye Res*. 2015;45:30–57. doi:10.1016/j.preteyeres.2014.11.004
11. Yan W, Sun Y, Wang Y, et al. The impacts of resveratrol on the retinal degeneration in a rat model of retinitis pigmentosa induced by alkylation: an in-vivo study. *Anim Cells Syst*. 2023;27(1):138–148. doi:10.1080/19768354.2023.2226695
12. Yan WM, Long P, Chen MZ, et al. Retinal neovascularization induced by mutant Vldlr gene inhibited in an inherited retinitis pigmentosa mouse model: an in-vivo study. *Int J Ophthalmol*. 2021;14(7):990–997. doi:10.18240/ijo.2021.07.05
13. Tao Y, Chen T, Fang W, et al. The temporal topography of the N-Methyl-N-nitrosourea induced photoreceptor degeneration in mouse retina. *Sci Rep*. 2015;5:18612. doi:10.1038/srep18612
14. Deng X, Ge J, He M, Gao Y, Zhong Z. Retinal electroretinogram and pathological morphological changes in rats with photoreceptor cell damage induced by different doses of MNU. *Chin J Pathophysiol*. 2008;2008(4):828–832.
15. Tao Y, Chen T, Fang W, et al. The comparative efficiency of intraperitoneal and intravitreous injection of hydrogen rich saline against N-Methyl-N-Nitrosourea induced retinal degeneration: a topographic study. *Front Pharmacol*. 2017;8:587. doi:10.3389/fphar.2017.00587
16. Campochiaro PA, Mir TA. The mechanism of cone cell death in Retinitis Pigmentosa. *Prog Retin Eye Res*. 2018;62:24–37. doi:10.1016/j.preteyeres.2017.08.004
17. Kang K, Tarchick MJ, Yu X, Beight C, Bu P, Yu M. Carnosic acid slows photoreceptor degeneration in the Pde6b(rd10) mouse model of retinitis pigmentosa. *Sci Rep*. 2016;6:22632. doi:10.1038/srep22632
18. Aziz MK, Ni A, Esserman DA, Chavala SH. Evidence of early ultrastructural photoreceptor abnormalities in light-induced retinal degeneration using spectral domain optical coherence tomography. *Br J Ophthalmol*. 2014;98(7):984–989. doi:10.1136/bjophthalmol-2013-304515
19. Pennesi ME, Michaels KV, Magee SS, et al. Long-term characterization of retinal degeneration in rd1 and rd10 mice using spectral domain optical coherence tomography. *Invest Ophthalmol Vis Sci*. 2012;53(8):4644–4656. doi:10.1167/iovs.12-9611
20. Hariri S, Tam MC, Lee D, Hileeto D, Moayed AA, Bizheva K. Noninvasive imaging of the early effect of sodium iodate toxicity in a rat model of outer retina degeneration with spectral domain optical coherence tomography. *J Biomed Opt*. 2013;18(2):26017. doi:10.1117/1.JBO.18.2.026017
21. Yoshizawa K, Kuro-Kuwata M, Sasaki T, et al. Retinal degeneration induced in adult mice by a single intraperitoneal injection of N-ethyl-N-nitrosourea. *Toxicol Pathol*. 2011;39(4):606–613. doi:10.1177/0192623311402221
22. Ohsawa K, Imai Y, Sasaki Y, Kohsaka S. Microglia/macrophage-specific protein Iba1 binds to fimbrin and enhances its actin-bundling activity. *J Neurochem*. 2004;88(4):844–856. doi:10.1046/j.1471-4159.2003.02213.x
23. Zeng HY, Zhu XA, Zhang C, Yang LP, Wu LM, Tso MO. Identification of sequential events and factors associated with microglial activation, migration, and cytotoxicity in retinal degeneration in rd mice. *Invest Ophthalmol Vis Sci*. 2005;46(8):2992–2999. doi:10.1167/iovs.05-0118

Journal of Inflammation Research Dovepress

Publish your work in this journal

The Journal of Inflammation Research is an international, peer-reviewed open-access journal that welcomes laboratory and clinical findings on the molecular basis, cell biology and pharmacology of inflammation including original research, reviews, symposium reports, hypothesis formation and commentaries on: acute/chronic inflammation; mediators of inflammation; cellular processes; molecular mechanisms; pharmacology and novel anti-inflammatory drugs; clinical conditions involving inflammation. The manuscript management system is completely online and includes a very quick and fair peer-review system. Visit http://www.dovepress.com/testimonials.php to read real quotes from published authors.

Submit your manuscript here: https://www.dovepress.com/journal-of-inflammation-research-journal